Resolution Analysis of a Polymethylmethacrylate Tapered Probe in Near-Field Terahertz Imaging

B. Zhu [1], G. He [1], J. Stiens [1,2], J. Van Erps [3], W. Ranson [1,2], C. De Tandt [1], H. Thienpont [3], and R. Vounckx [1]

[1] Department of Electronics and Informatics
Vrije Universiteit Brussel (VUB), Brussels, B-1050, Belgium
bzhu@etro.vub.ac.be, ghe@etro.vub.ac.be, jstiens@etro.vub.ac.be, wranson@etro.vub.ac.be, cdtandt@etro.vub.ac.be, rvounckx@etro.vub.ac.be

[2] SSET Department
IMEC, Kapeldreef 75, Leuven, B-3001, Belgium

[3] Department of Applied Physics and Photonics
VUB, Brussels, B-1050, Belgium
jurgen.van.erps@vub.ac.be, hthienpo@b-phot.org

Abstract ─ A Polymethylmethacrylate (PMMA) rectangular tapered probe with metal coating on the sides is analyzed as a near-field imaging probe at 100 GHz in Ansoft High Frequency Structure Simulator (HFSS). Normally, highly resistive silicon and sapphire, which are costly, are used as a near-field probe due to their low loss and high permittivity. PMMA near-field probe is usually used in Scanning Near-field Optical Microscopy (SNOM), which is made from PMMA optical fibers. We propose for the first time to use PMMA as a near-field probe in millimeter and Terahertz wave scanning near-field imaging applications. The geometrical optimization of the tapered probe is carried out on the basis of different coupling methods. The beam shape merging from the end of the tapered tip is analyzed. The operation efficiency of two-side tapered and four-side tapered probes has been compared in view of the fabrication technique. A knife edge is simulated in HFSS to define the lateral resolution. Longitudinal resolution is discussed through setting a stair step shaped sample. A high lateral resolution around the end of the probe size can be achieved and even higher longitudinal resolution. The impact of the tip-sample distance and the lateral resolution are clearly illustrated via simulations. Experiments are carried out using a two-side tapered probe provided with an aluminum coating. The resolution is defined by scanning a PMMA board which was half coated with aluminum.

Index Terms ─ Near-field, Polymethylmethacrylate tapered probe, Terahertz imaging.

I. INTRODUCTION

The history of the development of near-field optical microscopy shows that illumination techniques play an important role in the resolution improvement. An overview of sub-wavelength illumination and nano-metric shadowing [1] clearly illustrated the merits and demerits of lens-based microscopes, confocal imaging systems, and using a prism to create an evanescent field of radiation. In order to break the resolution limit, near-field scanning optical microscopy developed into aperture and aperture-less configurations. In the former, light is sent through an aperture that is much smaller than its wavelength and then the aperture or the sample are scanned relative to each other at a distance much smaller than a wavelength. The resolution of the aperture type near-field microscope always depends on the diameter of the aperture, and as such, the aperture fabrication technique is becoming the bottleneck for achieving the highest resolution. Much higher

Submitted On: October 30, 2013
Accepted On: September 28, 2014

resolutions are achieved by aperture-less type near-field imaging systems, which act as a scatterer converting the evanescent wave to propagation wave. In the millimeter and terahertz wave range, aperture type near-field imaging systems are always used in the lower frequency band. Coaxial probes, microstrip- and strip-lines, small circular and slit-like aperture in a conducting screen are the most commonly used probe-types in the microwave region [2-3]. A number of different aperture types such as a metal micro-slit probe [2-4], a metal-coated pyramidal silicon probe with a very small hole [5], and a tapered micro-strip gold line deposited on a ceramic alumina substrate [6] enabled a high resolution of the order of the dimension of the end of the probe. Even higher resolution (λ/2000) was obtained with an aperture-less probe such as a waveguide resonator coupled to a tapered metal probe [7], and the highest resolution (λ/3000) at 2.54 THz was achieved by using a single frequency source and a scattering tip [8]. Sharp metal tips acting like an antenna and strengthening the near-field signal below it, in combination with a lock-in technique applied in the near-field system, largely improve the resolution and the signal-to-noise ratio.

Although, the highest resolution was achieved by the aperture-less type solutions in near-field Terahertz wave microscopy, setting up an imaging system with a sharp metal needle which needs to keep the constant tip-sample distance, is not practicable for lowest frequency of the Terahertz waves for rough samples. Although, shear force is widely used in optical microscopy and at higher Terahertz wave frequency bands to keep the tip-sample distance constant in order to get nanometer resolution, but for micrometer resolution, it is not suitable.

In previous work [9-12], the tapered probe was designed in Teflon. Its coupling with a horn antenna through free space was combined with a tungsten needle close to the tapered probe to get a higher resolution. For a rectangular tapered probe, it is not material sensitive as we analyzed in [14]. The first use of PMMA optical fiber-made probes for SNOM has been reported in [13]. In this paper, we propose for the first time to use a rectangular tapered PMMA probe directly inserted into a standard rectangular metal waveguide to guide the Electromagnetic (EM) wave from the source onto the surface of the sample and record the reflection from it. Since PMMA is cheap, easy to process into a tapered probe and to apply the metal coating on it, we limited in this paper our resolution study to the impact of the probe's geometrical parameters. The optimization for a four-side and a two-side tapered probe is executed respectively in Section II with the emphasis on the fabrication tolerance. The resolution simulations are carried out in Section III, where we discuss the relationship between the tip-sample distance and the lateral resolution. The edge response is employed here to define the lateral resolution. The longitudinal resolution is defined by scanning a stair step shaped sample. The two-side tapered probes are fabricated and measured. Experimental results are shown in Section IV. The conclusions are drawn in Section V.

II. OPTIMIZATION OF THE FOCUSING TAPERED PROBE

A. Four-side tapered probe

There are four types of tapered probe for near-field imaging applications which can couple with standard rectangular waveguides. Figure 1 shows six probe types, we have analyzed in this paper, (a)-(d) are four-side tapered probes, according to different types of coating. These are respectively designated as FTTCN, FTTCW, FTFCN, and FTFCW, probes designed for different coupling modes. Figure 1 (e)-(f) are two-side tapered probes to discuss the influence of the fabrication technique. As illustrated in [14], two types of tapered probes were analyzed: one is a two-sided coated taper where only the narrow side of tapered parts are coated (FTTCN) [5], and the other one is a four-sided taper which has a metal coating on the full narrow sides (FTFCN) [15]. When an FTTCN type probe is inserted into a standard rectangular metal waveguide, the main mode TE10 changes to the dielectric waveguide mode and is gradually converted into a strip line mode where the electric field is confined between the two metallization pads. The FTFCN type probe directly converts the TE10 mode to a Quasi-TEM mode, which is the strip line mode. Due to the full metal coating on the narrow sides, the E-field direction is perpendicular to the narrow sides. Comparing these two kinds of probes, as illustrated by Fig. 1 (a) and (c), the FTFCN probe has a higher focusing intensity than the FTTCN probe. This narrow side coated probe can be inserted into a

standard rectangular waveguide, and when the probe is fixed just right in the end of the rectangular waveguide, the TE10 mode is still the main mode. The coating on the wide side can confine the E-field into a micro-strip line mode. Figure 2 shows a schematic picture of the tapered probe. The rectangular part has dimensions of $a \times b = 2 \times 1$ mm^2, which is convenient to couple with a standard rectangular metal waveguide WR-10 (2.54×1.27 mm^2) in the W-band (75 GHz - 110 GHz).

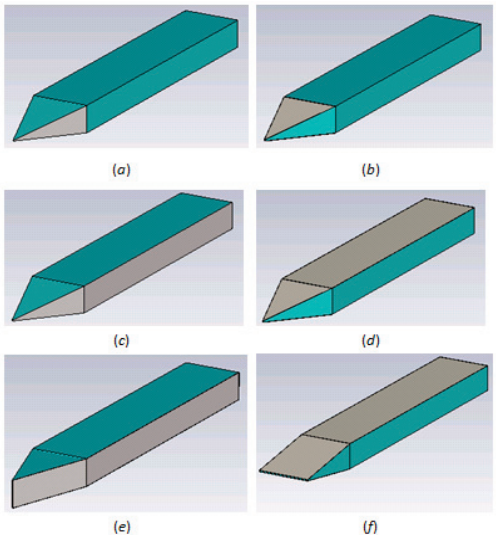

Fig. 1. Six types of tapered probes with a coating applied on different sides: (a) Four-side Tapered Two-side Coated on the Narrow tapered sides (FTTCN), (b) Four-side Tapered Two-side Coated on the Wide tapered sides (FTTCW), (c) Four-side Tapered Four-side Coated on the Narrow sides (FTFCN), (d) Four-side Tapered Four-side Coated on the Wide sides (FTFCW), (e) Two-side Tapered Four-side Coated on the Narrow sides (TTFCN), and (f) Two-side Tapered Four-side Coated on the Wide sides (TTFCW); the gray color is the metal coating, and the green color is the PMMA probe. The coating has been applied on the opposite side as well (but cannot be seen from this perspective view).

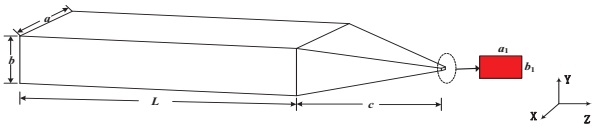

Fig. 2. A schematic picture illustrating the geometric dimensions.

The source which is used to excite the near-field probe is a TE10 mode, so the coating is applied on the wide side of the probe to confine the E-field. We choose a practical length for the rectangular part of the probe L=10 mm, and for the length of the taper we choose c=3 mm. From our optimization simulations in HFSS, this length allows focusing exactly at the end of the tip (the optimal aim is that the beam coming out from the taper can focus right at the end of the tip and the E-field intensity is the highest) when $a_1 \times b_1 = 0.02 \times 0.02$ mm^2. The permittivity of PMMA is 2.6, and its loss tangent is 0.003 at 100 GHz.

Figure 3 (a) shows the 2D E-field distribution in the vicinity of the end of the probe in the *xoz* plane, Fig. 3 (b) shows the distribution in the *yoz* plane, and Fig. 4 shows the E-field intensity along the *z* direction (x=0, y=0). It can be seen that there is good focusing at the end of the tip.

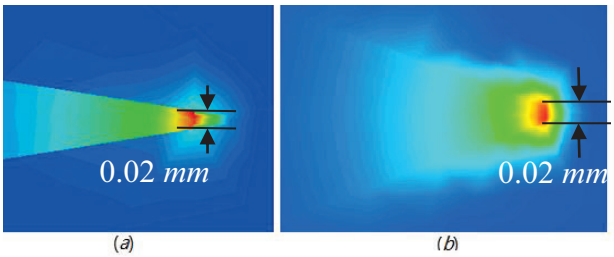

Fig. 3. 2D E-field distributions near the end of the probe for the four-side tapered probe: (a) in the *xoz* plane, and (b) in the *yoz* plane.

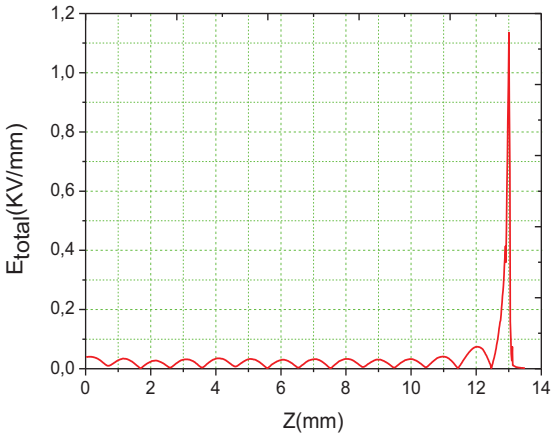

Fig. 4. E-field intensity along the *z* direction when x=0, y=0.

It can be observed from Fig. 4 that the E-field intensity quickly decays near the end of the tip.

Fitting the evanescent E-field intensity curve beyond the end of the tip with $z \geq 13$ mm using a general exponential function, $f(x)=a\exp(bx)$, in MATLAB, yields the following values for a and b respectively, a=1.741×10173 (KV/mm) which can be considered as positive infinite and b=-30.66 (KV/mm), the E-field intensity drops close to 0 in 100 μm beyond the end of the tip.

B. Two-side tapered probe

Since there are always some fabrication tolerances to take into account and a two-side tapered probe such as illustrated in Fig. 1 (e) and (f) is much easier to fabricate, we investigate the influence of a variation of parameters a_1 and b_1. First, we fix a_1=2 mm and change b_1. The metal coating is applied on the wide side since the launched mode is TE10. Fixing b_1=1 mm and changing a_1 makes no sense since the E-field is not in that direction. When b_1=0.0175 mm, the optimized beam shape is achieved.

Figure 5 shows the detailed E-field distribution near the end of the probe. In the *yoz* plane, we see that the beam size is around the dimension of the end of the probe; i.e., 0.0175 mm wide and quickly decaying. In the *xoz* plane, we observe 1 mm beam size (Full Width at Half Maximum (FWHM)). It should be noted that it is still nessesary to use a four-side taper to get smaller beam size and higher E-field intensity. Figure 6 shows the E-field intensity along the *z* direction at x=0, y=0. The maximum intensity is 0.264 KV/mm, which is only 23% of the maximum E-field intensity achieved with an optimized four-side tapered probe in Fig. 3. For the ease of fabrication, however, we opt for a two-side tapered probe for our experiments since it also shows field focusing in the end of the tip.

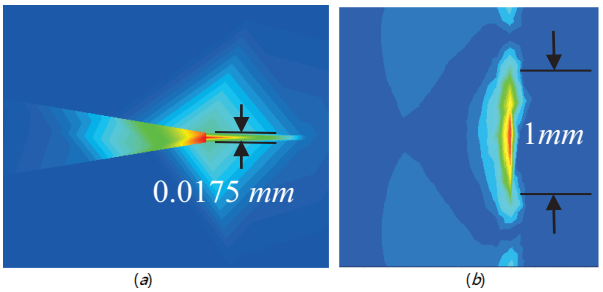

Fig. 5. 2D field distribution at the end of the probe for the wide-side tapered probe: (a) in the *xoz* plane, and (b) in the *yoz* plane.

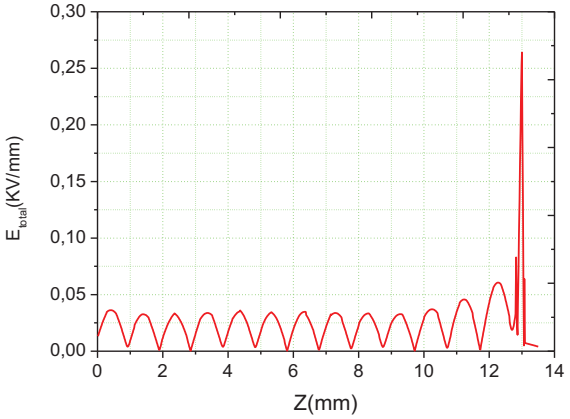

Fig. 6. E-field distribution in the end of the two-side tapered probe.

III. RESOLUTION SIMULATIONS

In Terahertz wave microscopy, the spatial resolution is always defined by the "Line Spread Function" (LSF) and the "edge response." The LSF is the response of the setup to a thin line-shape object across the light path. Similarly, the edge response is what one measures when a sharp straight discontinuity, an edge for example, is placed into the light path of the setup. Since a line is the derivative of an edge, the LSF is the derivative of the edge response in a linear system. Edge resolution is then defined as the lateral displacement with a change from 10 to 90% of the optical signal over an edge [16].

Figure 7 shows the model in HFSS, where the waveguide port source is placed at the end of the rectangular part. A sample is positioned closely to the end of the tip. The tip-sample distance is *d*, the metal plate is 0.1 mm thick and 1 mm wide. The sample is scanned from left to right. The reflection parameter S_{11} is measured. We record the data from -25 μm to +25 μm. The tapered probe used is the optimized one ($a \times b$=2×1 mm^2, L=10 mm, c=3 mm, $a_1 \times b_1$=0.02×0.02 mm^2); the beam size is around 0.02 mm (λ/150) at 100 GHz.

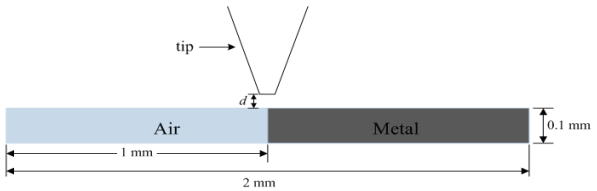

Fig. 7. Geometrical model of tip and sample.

From the simulation results shown in Fig. 8,

we can see that when the tip-sample distance is d=0 mm, one can clearly distinguish the edge from the phase, magnitude, real and imaginary part of S_{11} information. The edge is sharper in the real part information than in the imaginary one. There is around 20 μm for the 10 to 90% edge in the imaginary part information, from which we can conclude that the imgainary part cannot get a higher resolution than the size of the probe itself. Phase and magnitude information also have a 20 μm shift which exactly corresponds to the size of the tip. When the tip is scanned over the sample from left to right, the right side of the probe touches the metal edge when the probe's center point is at position -10 μm. This means that the phase information changes immediately when the probe edge touches the metal edge. The magnitude also contains the information about the beam size. When the probe goes across the edge, 20 μm beam size is shown in the process of the scanning; when the probe is located completely above the metal plate, the sharp edge effect starts. Therefore, the phase information is more sensitive than the magnitude information. The position of the phase change is right at the position where the edge is placed. The position of the magnitude change is equal to the edge position plus the beam size. In one word, the size of the beam or the dimension of the end of the probe leads to the 20 μm lag of the magnitude.

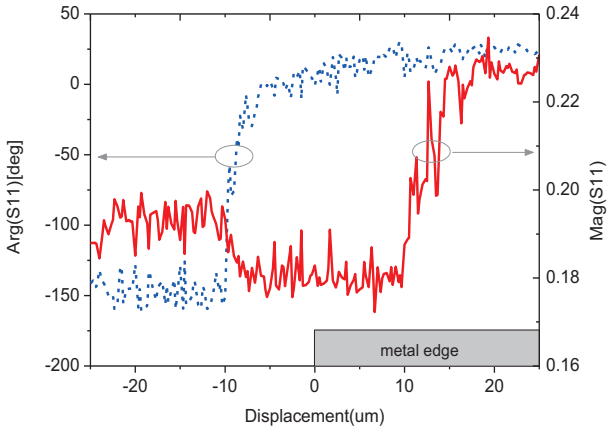

(a)

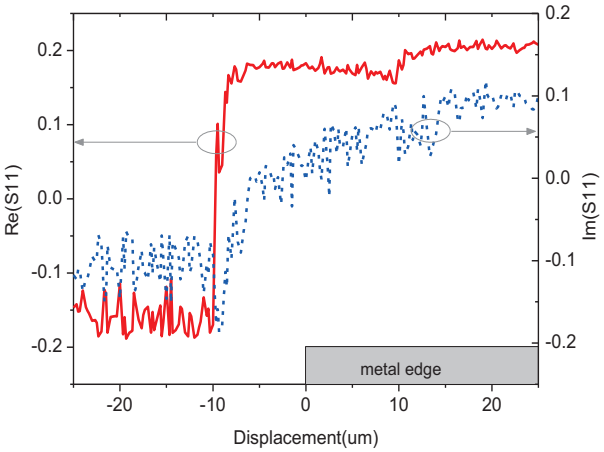

(b)

Fig. 8. Simulated reflection using a linear scanning for a tip-sample distance d=0 mm: (a) phase and magnitude, and (b) real and imaginary part of S_{11}.

Figure 9 shows the impact of the distance d for d=0, 10, 20, 100, 200, 500, 1000 nm on the phase, magnitude, real part and imaginary part of S_{11} during the linear scan of the edge. The smaller the distance, the higher the resolution is. When d is 100 nm, the edge is not sharp anymore. For d>100 nm, the edge fades away when the probe is scanned above the metal plate. Hence, in the experimental setup, one is obliged to keep the tip-sample distance d at sub-100 nm level.

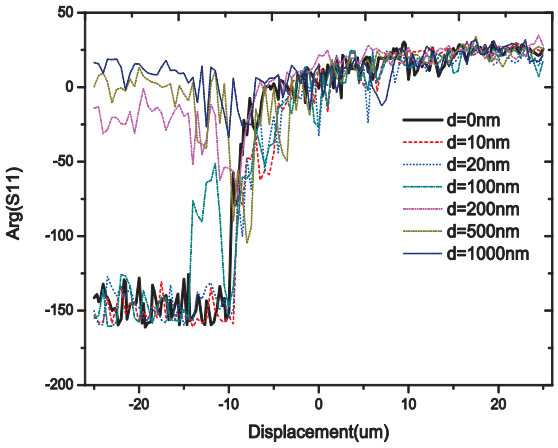

(a)

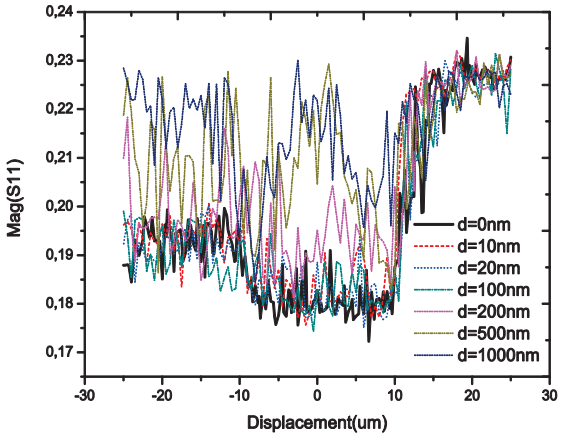

(b)

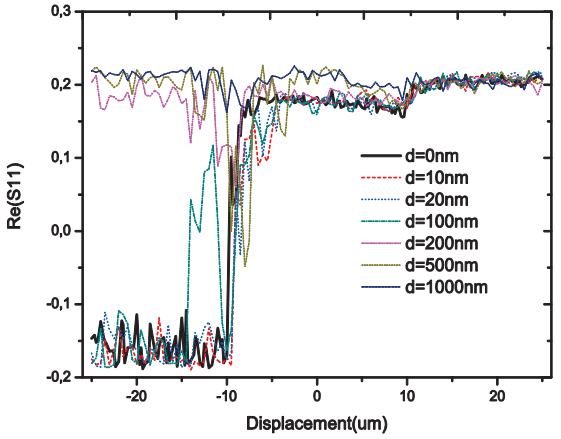

(c)

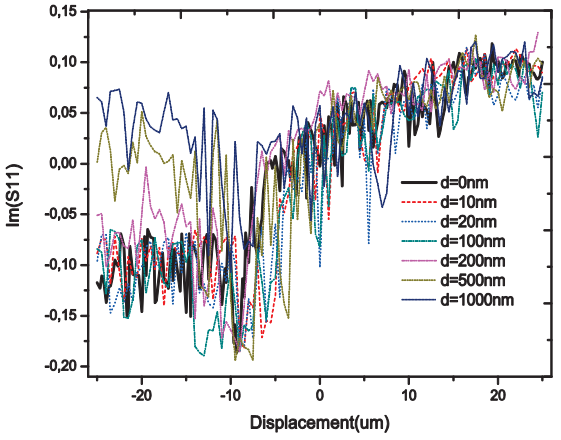

(d)

Fig. 9. Simulated reflection for a linear scanning when the tip-sample distance d=0, 10, 20, 100, 200, 500, 1000 nm: (a) phase, (b) magnitude, (c) real part, and (d) imaginary part of S_{11}.

The tip-sample distance is a key factor for the lateral resolution; the smaller the tip-sample distance, the higher the lateral resolution. The highest resolution can be extrated from the phase and magnitude and real part information of S_{11}. From those, we can get a 5 μm (λ/600) edge resolution which is 1/4 of the size of the end probe; whereas, the imaginary part cannot yield a higher resolution than 20 μm (λ/150), which is the size of the end probe when the tip-sample distance is d=0 nm. Since the phase information is most sensitive of all, phase measurements are suggested in the experiment.

In order to observe the longitudinal resolution, we make use of a stair step sample which is shown in Fig. 10. Here, the tip-sample distance is d, and step height is h. We set h as small as 500 nm (λ/6000), and d=0 nm. From the results in Fig. 11, showing the phase, magnitude, real part and imaginary part information of S_{11}, we can see the 0.5 μm step. Higher longitudinal resolution may abtained in the simulation by setting a smaller h. It costs too much computer memory to set a finer mesh and do the scanning for the resolution simulations. Therefore, λ/6000 is achievable based on the limited simulation environment.

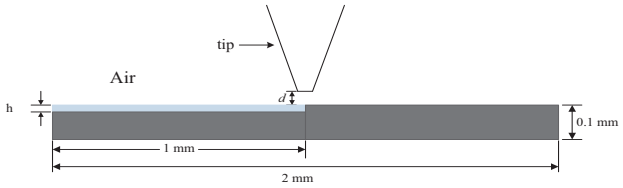

Fig. 10. Longitudinal resolution simulation model.

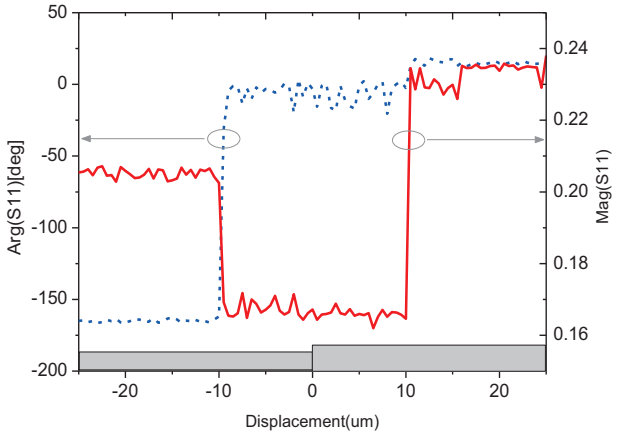

(a)

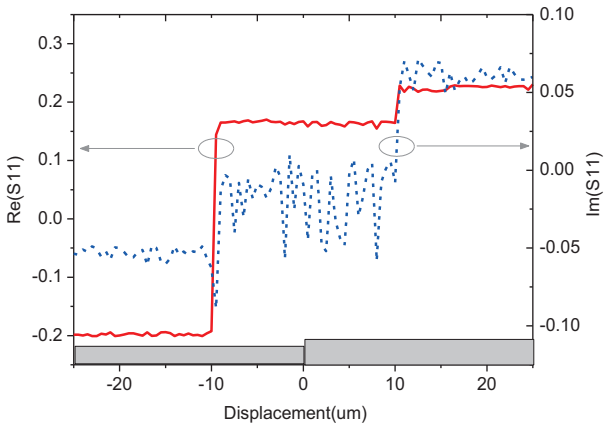

(b)

Fig. 11. Simulated reflection for the stair step sample when the step height h is equal to 0.5 μm.

IV. EXPERIMENTAL RESULTS

The two-side tapered probes were machined using a VHF CAM-100 micro-milling station. The material is PMMA of 1 mm thickness, which is sold by Notz Plastics AG under the brand name Topacryl/Hesaglas. A double-tooth carbide cutter tool with a diameter of 0.5 mm was used for the micro-machining. The resulting surface roughness of the micro-machined probe sidewalls was characterized using a non-contact optical surface profiler WYKO NT-2000 (Bruker). A root-mean-square surface roughness (Rq) of about 1 μm was measured over a surface area of 175 μm × 230 μm. An example of a measured surface profile is shown in Fig. 12 (a). This roughness is sufficiently low for this appliction at 100 GHz. TTFCN and TTFCW probes, as illustrated schematically in Fig. 1 (e) and (f), were fabricated and an evaporated aluminum coating around 600 nm thick had applied subsequently. For the evaporated aluminum coating, the uncoated parts have to be protected. Plastic tape is used to protect the sided and the end facet. Since the end facet is very small, the exact protection is quite difficult. If the tape protected area is bigger than the end facet area and covers the tapered sides, the joint line of the end facet is and the tapered sides is not sharp and there is no coating on the protected part. The end facet of the TTFCN probe is 100 μm width without aluminum coating observed with a JEOL JSM-6400 scanning electron microscope in Fig. 12 (b). The protection of the end facet of the tip during the coating application is not exact enough and there is also around 100 μm width in the sides of the probe did not cover by the metal coating. The end detail of the TTFCW probe is shown in Fig. 12 (c), the target width is 0.0175 mm and also the protection of the end facet is hard, the wide tapered sides do not have the sharp coating edge.

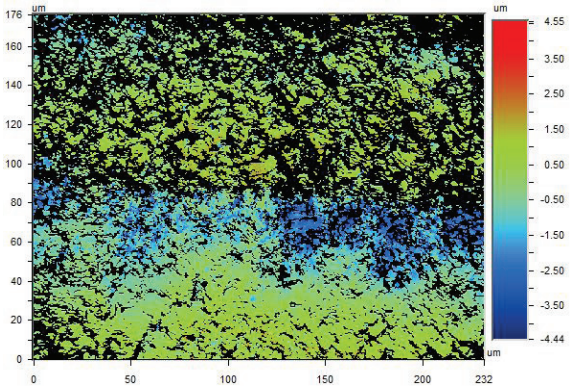

(a)

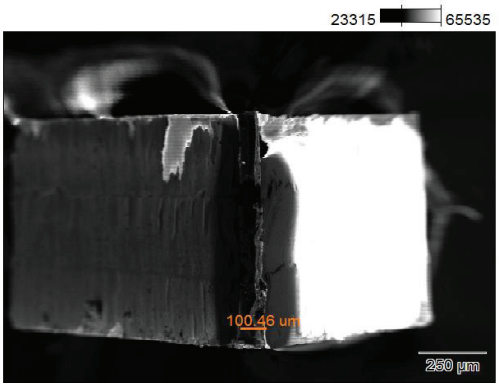

(b)

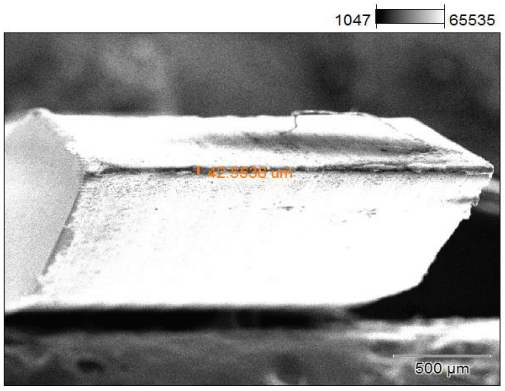

(c)

Fig. 12. (a) Measured surface profile of the micro-milled surfaces of the tapered probe, (b) image of the end of the tapered probe for TTFCN with a_1=0.098 mm, and (c) image of the end of the tapered probe for TTFCW with b_1=0.0175 mm.

The imaging setup is shown in Fig. 13, the block diagram of the imaging system and a photograph of the experimental setup, respectively. The EM wave is generated by a Backward Wave Oscillator (BWO) source sweep generator G4403E from Elmika, with a frequency range from 75 GHz to 110 GHz and accuracy around ±0.2%. Its output power can reach 15 mW over the whole band. We set it to a fixed frequency of 100 GHz in the experiments. A Directional Coupler (DC) is used after the output of the G4403E, and an FTL WDP-10 from Farran is used as reflection power detector. This detector employs finline technology and zero biased beamlead Schottky barrier diodes. The WDP-10 works from 75 to 110 GHz, and its sensitivity is typically bigger than 550 mV/mW. We used an E-Bender (EB) to change the horizontal direction to vertical direction, and a Straight Waveguide (SW) to extend the length. The PMMA Tapered Probe (TP) is coupled with the SW. The end of the probe is contacted with the sample since it is difficult to control the tip-sample distance in the nanometer range. The rectangular PMMA sample which is mounted on the *xy* stage is half coated with aluminum to make an edge effect. Two types of the coupling mode have been tested in the experimental setup. One is using the TTFCN probe which is inserted into the SW, and the other one is using the TTFCW probe which is fixed at the end of the SW. Reflection is observed through this setup.

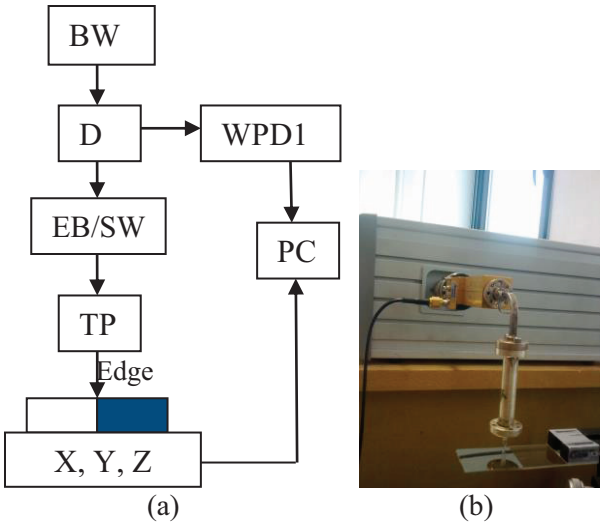

Fig. 13. (a) Block diagram of the imaging setup, and (b) photograph of the experimental.

We scan the sample from the aluminum coated part to the uncoated part. The measurement results are shown in Fig. 14, where the scanning range is 8000 μm, and each step is 100 μm, using the 10% to 90% edge function. Figure 14 (a) shows the results for the TTFCN probe and (b) depicts the results for the TTFCW probe. It is observed that the edge width is around 1.12 mm and 0.75 mm respectively. The TTFCN probe has an $a_1 \times b_1 = 0.1 \times 1$ mm^2 end facet and the measured edge width is around 1 mm, which is the wide size of the end of the taper. The TTFCW probe has an $a_1 \times b_1 = 2 \times 0.0175$ mm^2 end facet and the measured edge width is around 0.75 mm, which is bigger than the beam size (0.0175 mm) in the *yoz* plane and less than the beam size (1 mm) in the *xoz* plane. Since the simulations are carried out in the ideal conditions which are different from the experimental environment, especially for the aluminum coating of the probes which are shown in Fig. 12 (b) and (c), the uncoated area on the tapered sides exists as the protection for a small facet is quite difficult. The probe and standard waveguide connection impacts the results as well since the designed probe is smaller than the standard waveguide WR-10, two types of the coupling modes are different from the ideal simulations. The differences between the experimental results and simulation results are reasonable and understandable. Because the detector can only measure the power, the phase information is not available, and hence, the potentially most sensitive way of measuring has not yet been verified experimentally.

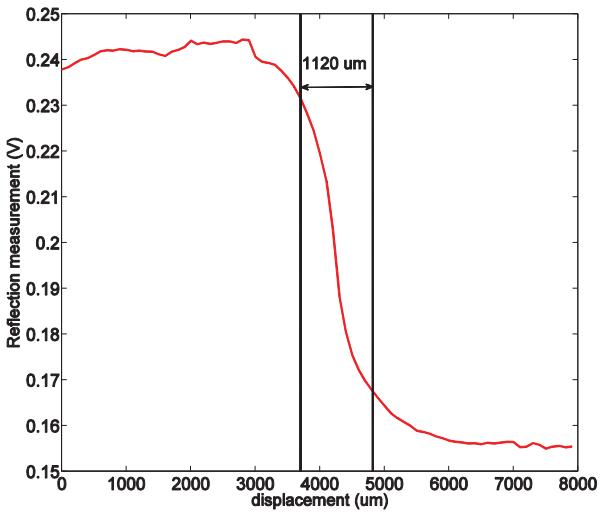

(a)

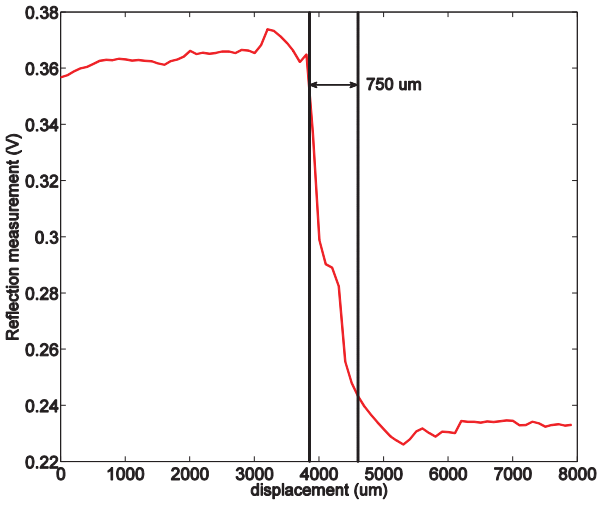

(b)

Fig. 14. Experimentally measured edge effect: (a) for the TTFCN probe, and (b) for the TTFCW probe.

V. CONCLUSION

This paper proposes for the first time the use of PMMA near-field probes to replace the costly low loss and high permittivity materials such as silicon and Sapphire, which are generally used for this purpose in millimeter and Terahertz wave imaging applications. A good field concentration in the end of the tapered probe is obtained by applying a metal coating on the PMMA probe. The coating area can be designed according to the coupling mode. When the tapered probe is totally inserted into a standard wave guide, a QTEM mode is excited in the tapered probe when its narrow side is coated. If the tapered probe is fixed in the end of a standard waveguide, a TE10 mode exists in the tapered probe if its wide side is coated. An optimization was carried out for the FTFCW and TTFCW probe. Simulations to determine the achievable lateral and longitudinal resolution have been performed for an edge (metal plate) and a stair step sample scanned with the FTFCW probe by examining the S_{11} parameters. We found that the phase information is most sensitive, and that a resolution of $\lambda/600$ laterally and at least $\lambda/6000$ longitudinally can be reached in the simulations. The TTFCN and TTFCW probes were fabricated by micro-milling and an aluminum coating was applied by evaporation. Experiments were carried out with a BWO source. The edge effect was observed and the measured results were analyzed. The resolution of 1.12 and 0.75 mm was obtained for TTFCN and TTFCW probes, respectively.

ACKNOWLEDGMENT

This work has been partially funded by FWOAL682 “Building blocks of lab-on-chip system for label-free monitoring of biomolecular interactions,” by the Industrial Research Fund of VUB, IOF242, by the Strategic Research Program of VUB, SRP-M3D2, and by the IMEC BISENS laboratory. This work is also executed in the framework of NEWFOCUS ESF Research Networking Program (RNP). J. Van Erps was supported by the FWO Vlaanderen under a post-doctoral research fellowship.

REFERENCES

[1] A. Lewis, “Near-field optics: from subwavelength illumination to nanometric shadowing,” *Nature Biotechnology*, vol. 21, no. 11, pp. 1378-1386, 2003.

[2] T. Nozokido, T. Ohbayashi, J. Bae, and K. Mizuno, “A resonant slit-type probe for millimeter-wave scanning near-field microscopy,” *IEICE Trans. Electron.*, vol. E87-C, no. 12, 2004.

[3] T. Nozokido, S. Nuimura, T. Hamano, J. Bae, and K. Mizuno, “A new object mounting structure for use in millimeter-wave scanning near-field microscopy,” *IEICE Trans. Electron.*, vol. 1, no. 6, 144-149, 2004.

[4] J. Bae, T. Okamoto, T. Fujii, and K. Mizuno, “Experimental demonstration for scanning near-field optical microscopy using a metal micro-slit probe at millimeter wavelengths,” *Applied Physics Letters*, vol. 71, no. 24, pp. 3581-3583, 1997.

[5] N. Klein, P. Lahl, and U. Poppe, “A metal-dielectric antenna for terahertz near-field imaging,” *Journal of Applied Physics*, vol. 98, no. 014910, 2005.

[6] O. Benzaim, K. Haddadi, M. M. Wang, D. Maazi, and T. Lasri, “Scanning near-field millimeter-wave microscope: application to a vector-coding technique,” *IEEE Transaction on Instrumentation and Measurement*, vol. 57, no. 11, pp. 2392-2397, 2008.

[7] M. Kim, J. Kim, H. Kim, S. Kim, J. Yang, H. Yoo, S. Kim, K. Lee, and B. Friedman, “Nondestructive high spatial resolution imaging with a 60 GHz near-field scanning millimeter-wave microscope,” *Review of Scientific Instruments*, vol. 75, no. 3, pp. 684-688, 2004.

[8] A. J. Huber, F. Keilmann, J. Wittborn, J. Aizpurua, and R. Hillenbrand, “Terahertz near-field

nanoscopy of mobile carriers in single semiconductor nanodevices," *Nano Letters*, vol. 8 no. 11 pp. 3766-3770, 2008.

[9] B. Zhu, S. Vanloocke, J. Stiens, D. De Zutter, and R. Vounckx, "A novel 3D printed focusing probe in scattering-type scanning near-field millimeter and terahertz wave microscope," *European Conference on Antennas and Propagation*, Rome, Italy, pp. 775-778, 2011.

[10] B. Zhu, J. Stiens, G. Poesen, S. Vanloocke, D. De Zutter, and R. Vounckx, "Dielectric analysis of 3D printed materials for focusing elements operating in Mm and THz wave frequency bands," *Proceedings of Symposium IEEE/LEOS Benelux Chapter*, Delft, Netherland, pp. 13-16, 2010.

[11] B. Zhu, S. Vanloocke, V. Matvejev, J. Stiens, D. De Zutter, and R. Vounckx, "Scanning near-field millimeter wave microscope combining dielectric tapered probes and metal tips," *Progress In Electromagnetics Research Symposium*, Suzhou, China, pp. 12-16, September 2011.

[12] B. Zhu, J. Stiens, V. Matvejev, and R. Vounckx, "Inexpensive and easy fabrication of multimode tapered dielectric circular probes at millimeter wave frequencis," *Progress In Electromagnetics Research*, vol. 126, pp. 237-254, 2012.

[13] H. Chibani, K. Dukenbayev, M. Mensi, S. K. Sekatskii, and G. Dietler, "Near-field scanning optical microscopy using polymethylmethacrylate optical fiber probes," *Ultramicroscopy*, vol. 110, pp. 211-215, 2010.

[14] B. Zhu, G. He, J. Stiens, and R. Vounckx, "Analysis and optimization of a focusing metal-dielectric probe for near field terahertz imaging," *EuMW2013*, Nuremberg, Germany, pp. 6~11, October 2013.

[15] M. Berta, P. Kuzel, and F. Kadlec, "Study of responsiveness of near-field terhertz imaging probes," *J. Phys. D: Appl. Phys.*, vol. 42, 2009.

[16] R. A. J. L. Adam, "Review of near-field terahertz measurement mehtods and their applications," *J. Infrared Milli. Terahz. Waves*, vol. 32, pp. 976-1019, 2011.

Bin Zhu received the B. E. degree in Electronics and Information Engineering from Harbin Engineering University, Harbin, China, in 2004, the M. S. degree in Communication and Information System from Dalian University of Technology, Dalian, China, in 2006, and the Ph.D. degree in Vrije Universiteit Brussel, Brussels, Belgium in 2014. Her research interest is focused on near-field imaging, non-destructive testing and dielectric spectroscopy.

Guoqiang He received the B. E. degree in Vacuum Electronic Technique from the University of Electronic Science and Technology of China (UESTC), Chengdu, China, in 2010, and the M. S. degree in Radio Physics from UESTC, Chengdu, China, in 2013. Currently, he is working towards the Ph. D. degree in Electrical Engineering at Vrije Universiteit Brussel (VUB), Brussels, Belgium. His current research interest is in millimeter wave and Terahertz detectors.

Johan Stiens received the Electromechanical Engineering degree with majors in Applied Physics and the Ph.D. degree (with greatest honors) from the Faculty of Engineering Sciences, Vrije Universiteit Brussel (VUB), Brussels, Belgium, in 1990 and 1996, respectively.

He is currently with VUB. His current research interests include semiconductor physics and technologies, including micromachining for microfluidics, optoelectronic devices, plasmonics, metamaterials and devices, and systems for active (near-field) imaging and sensing in the millimeter and terahertz (THz) wave domain. He is the author or coauthor of about 180 international journal and conference papers. He owns eight patents and four pending patents. He is a Reviewer of several scientific journals and has been elected as an expert for the evaluation of research grants, and national and international scientific/industrial projects. He has been a Consultant for several years for companies and research institutes. Since January 2012, he has been a "Professor." Besides his technical teaching, he is also involved in entrepreneurship courses, merging technical and business engineers. He was a Cofounder of the spin-off company Ecologic, dealing with equalizer chips.

Jürgen Van Erps was born in Etterbeek, Belgium, in 1980. He graduated as an Electrotechnical Engineer with majors in Photonics at the Vrije Universiteit Brussel (VUB) in 2003 and obtained his Ph.D. summa cum laude at the same university in 2008.

Since February 2013, he is a Part-time Professor at VUB, teaching an introductory course on Photonics and

a course on Optical Communication Systems. In 2009 and 2010, he was a Visiting Researcher at the Centre for Ultrahigh bandwidth Devices for Optical Systems (CUDOS) at the University of Sydney, Australia, under an Erasmus-Mundus Action 3 scholarship of the European Union. His research there involved high-resolution optical sampling of ultrahigh bitrate signals using dispersion-engineered highly nonlinear chalcogenide waveguides, and automatic dispersion monitoring and compensation of 1.28Tbaud links. Currently, he is continuing his research at VUB on the modeling of micro-optical systems for optical interconnects and optofluidics applications, and their fabrication by means of Deep Proton Writing, ultraprecision diamond tooling and hot embossing. He is also involved in experimental work on nonlinear optics in integrated photonic devices. He was Invited Speaker at several international conferences. He authored or co-authored 32 SCI-stated papers and more than 80 papers in international conference proceedings. He is co-inventor of 2 patents. He serves as a Reviewer for several international journals. He is a Senior Member of the SPIE, and Member of the OSA and the IEEE Photonics Society. He was also co-founder and 2006-2007 President of the SPIE Brussels Student Chapter.

Willy Ranson received the Telecommunication Engineer degree in 1975 from the University of Leuven, Belgium. He was Assistant Professor in the Department of Microwaves and Lasers at the University of Leuven until 1983, when he joined the Department of Electronics and Information Processing (ETRO) of the Vrije Universiteit Brussel (VUB).

Since 1990, he has been a Member of the Inter-university Micro-Electronics Center (IMEC) in the VUB. Ranson has participated in projects and contracted research on such diverse topics as planar antenna structures, high frequency wave-guides, chemical sensors, biological applications for breast cancer detection, optical information processing for parallel computation, CO2 laser applications, microelectronic process technology and revolutionary information and revolutionary computation theories. He is currently Senior Researcher in charge of the processing technology lab of LAMI and is a Founder Member of LIFE (Living Systems). His current research contributions are in the areas of CO2 laser modulation, millimeter imaging systems, micro machines for ultra-rapid DNA screening, fast enforcing technologies for protein engineering and Evolutionary Living Systems. Ranson is (co)author of more than 140 publications in international refereed journals and conferences.

Cathleen De Tandt graduated at the Industrial High School for Engineering of Ghent (C.T.L), in 1979, as an Industrial Engineer in Chemicals. She was teaching chemistry until 1981, and from 1982 she was working at the Vrije Universiteit Brussel-Jette together with Dr. Rogiers in the area of mucoviscidose.

In 1983, she worked as Technologist at the Vrije Universiteit Brussel in the department of Electronics and Information Processing (ETRO-LAMI). From1984 till the end of December 2008, she was a Member (Research Engineer) of the Inter University Micro Electronic Center (IMEC) with a working place on the VUB Campus. Since January 2009, she's been working as Technologist at the Vrije Universiteit Brussel in the department of Electronics and Information Processing (ETRO-LAMI).

She has participated in projects on diverse topics as: chemical gas sensors, optical information processing for parallel computation, CO2 laser applications and modulation, microelectronic process technology, field emission devices, millimeter wave monitoring, technology for half conductive Coupling, technology for Infra-Red modulators, micro-machines for ultra-rapid DNA and protein screening, fast enforcing technologies for protein engineering. She is also a co-worker for Eqcologic, a spin-off of the ETRO-LAMI-group.

Hugo Thienpont (M'99) was born in Ninove, Belgium, in 1961. He graduated with the academic degree of Electrotechnical Engineering in 1984 and received the Ph.D. degree in Applied Sciences in 1990, both from the Vrije Universiteit Brussel (VUB), Brussels, Belgium. In 1994, he became Professor at the Faculty of Applied Sciences, with teaching responsibilities in photonics. In 2000, he became Research Director of the Department of Applied Physics and Photonics at the VUB, and in 2004, he was elected Chair of the department. Currently, he is the Coordinator of several basic research and networking projects such as the European Access to Micro-Optics Expertise, Services and Technologies (ACTMOST) network. In addition to academic oriented research projects, he manages microphotonics related industrial projects with companies like Barco, Agfa-Gevaert, Tyco, and Umicore. He authored more than 220 SCI-

stated journal papers and over 400 publications in international conference proceedings. He edited 15 conference proceedings, authored 7 chapters in books, and is co-inventor of 15 patents. Thienpont was Guest Editor of several special issues on Optical Interconnects for Applied Optics and the IEEE Journal of Selected Topics in Quantum Electronics. He is the General Chair of the International Society for Optical Engineers (SPIE) Photonics Europe conferences in Strasbourg and Brussels. In 1999, he was the recipient of the International Commission for Optics Prize and the Ernst Abbe medal from Carl Zeiss. In 2003, he was awarded the title of IEEE Laser and Electrooptics Society (LEOS) Distinguished Lecturer. He was also the recipient of SPIE President's Award in 2005 for dedicated service to the European Community and the international Micro-Optics Conference Award in 2007. He was an Invited Speaker at 50 international conferences. He is a Fellow of SPIE and EOS, and a Member of the Optical Society of America, and the IEEE Photonics Society.

Roger Vounckx was born in Brussels, Belgium, on June 26, 1952. He received the Dr. Sc. degree in Physics from the Electronics Department, Vrije Universiteit Brussels (VUB), Brussels, in 1984.

From 1975 to 1980, he was a Teaching Assistant of Faculty for Sciences in the Physics Department, VUB, where he became an Associate Professor of Microelectronics in 1984 and a Full Professor in 1993. During 1978-1979, he was engaged in military service. He became the Director of the Laboratory of Micro- and Photonelectronics (LAMI) in 1987, and the Head of the Electronics and Informatics Department (ETRO) in 2008. In 1988, he started a close collaboration with the Inter-University Microelectronics Centre (IMEC), Leuven, Belgium, and in 1998, LAMI became an associated research laboratory of IMEC's. He is currently with VUB. His current research interests include semiconductor devices and systems for optical and electrical information processing and communication and millimeter-wave imaging systems. He has authored or coauthored more than 250 technical papers in international journals and conference proceedings, and holds eight international patents. He was a Reviewer for international scientific journals and is an expert for evaluation of industrial research projects for the Belgian Government. He is currently involved in research of mid-infrared optoelectronics, artificially created living systems for truly intelligent computing, and a "Strategic Basic Research" Program from the Flemish Government for millimeter-wave imaging applications. He is a Cofounder and an Executive Director of EqcoLogic NV, LAMI's first spin-off company, which designs and produces silicon chips for fast data communication. Vounckx was the Chairman and a Member of program committees for international conferences.